Available online at www.sciencedirect.com
ScienceDirect
Coordination Chemistry Reviews 251 (2007) 351–363
COORDINATION CHEMISTRY REVIEWS
www.elsevier.com/locate/ccr

Review

Absorption spectroscopy of octahedral nickel(II) complexes: A case study of interactions between multiple electronic excited states

Emmanuel González, Alexandre Rodrigue-Witchel, Christian Reber *

Département de Chimie, Université de Montréal, Canada

Received 8 May 2006; accepted 9 August 2006
Available online 22 August 2006

Contents

Abstract

Absorption spectra of octahedral nickel(II) complexes are used to illustrate that the limitation to only the initial and Born–Oppenheimer final states of an electronic transition is not adequate in order to rationalize the intensity and vibronic structure of the lowest-energy spin-forbidden transition of these compounds. Qualitative and quantitative models are applied and discussed for a series of absorption spectra measured in solution at room temperature and for the low-temperature single-crystal absorption spectra of nickel(II) ions doped into bromide host lattices. The spectra and models illustrate the influence of multiple allowed transitions on the lowest-energy spin-forbidden band.

Keywords: Nickel(II) complexes; Solution absorption spectra; Polarized single-crystal absorption spectroscopy; Vibronic structure; Theoretical models; Coupled electronic states; Interference effects

1. Introduction

The rich electronic structure of octahedral nickel(II) complexes has been explored over the past 50 years towards goals ranging from applying crystal field theory in inorganic coordination chemistry [1–3] to modern photophysical effects such as near-infrared to visible upconversion [4]. The d–d transitions observed in the absorption spectra provide the crucial experimental information needed to develop and test models and concepts for these areas. All electronic states arising from the d^8 electron configuration in O_h point group symmetry are shown in the Tanabe–Sugano diagram in Fig. 1. The most important excited states discussed in this review are the $^3T_{2g}$, $^3T_{1g}(^3F)$ and the ^1E_g states. The energy of the first singlet excited state, ^1E_g, is almost independent of ligand-field strength, as it arises from the same $t_{2g}^6e_g^2$ electron configuration as the electronic ground state. In contrast, the energies of the triplet excited states vary strongly with ligand field strength, due to their electron configurations with an increased population of the E_g orbitals. The d^8 configuration is particularly attractive for this review, as the $^3T_{2g}$ and $^3T_{1g}(^3F)$ excited states are close in energy at all ligand-field strengths. The main focus is on the electronic states in the oval zone in Fig. 1, containing only one singlet excited state and two nearby triplet excited states. Absorption

* Corresponding author. Tel.: +1 514 343 7332; fax: +1 514 343 7586.
E-mail address: reber@chimie.umontreal.ca (C. Reber).

0010-8545/$ – see front matter © 2006 Elsevier B.V. All rights reserved.
doi:10.1016/j.ccr.2006.08.011

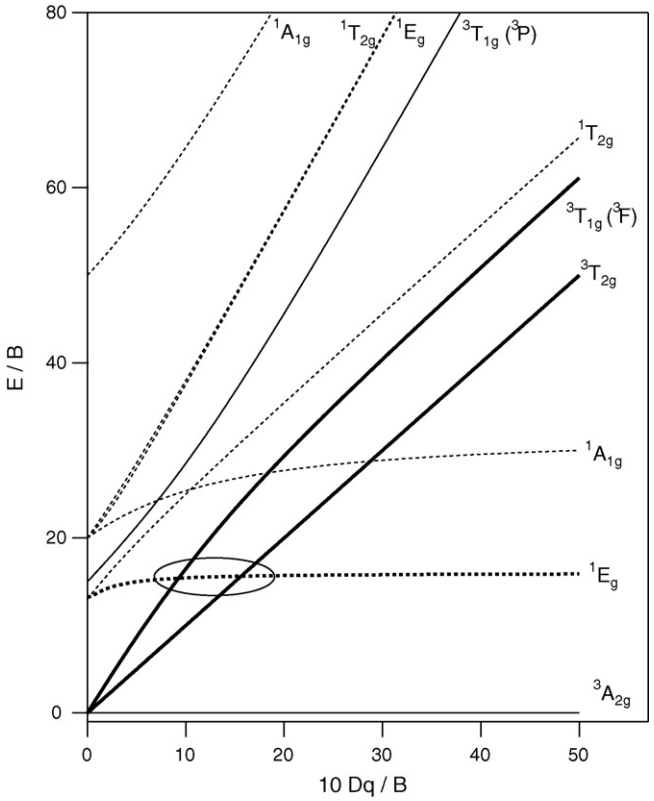

Fig. 1. Tanabe–Sugano diagram for the d^8 electron configuration in O_h point group symmetry. Triplet and singlet electronic states are given as solid and dotted traces, respectively, with excited states relevant to this review emphasized as thick traces. The oval denotes the energy and ligand-field strength range for which spectra are analyzed.

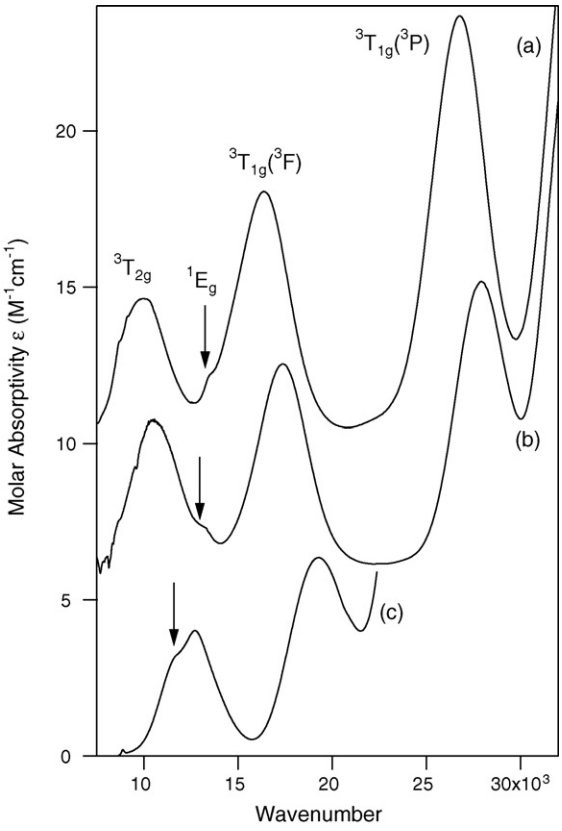

Fig. 2. Solution absorption spectra of: (a) $[Ni(imidazole)_6]^{2+}$, (b) $[Ni(NH_3)_6]^{2+}$, and (c) $[Ni(bipyridine)_3]^{2+}$. Traces (a) and (b) are offset along the ordinate for clarity. Vertical arrows denote the lowest-energy spin-forbidden transition to the ^1E_g excited state.

spectra covering this zone have been published and transition energies have been analyzed [1,3,5,6]. In the following, we discuss the intensity of the lowest-energy spin-forbidden transition, applying recently developed theoretical models [7,8]. The most important insight resulting from this review is that a forbidden transition close in energy to several allowed bands can lose or gain intensity compared to a situation where only a single allowed band is present and an intensity gain always occurs. The absorption spectra reviewed in the following show that intensity borrowing from several allowed bands is not additive, an effect often neglected when "mixed" wavefunctions of excited states are analyzed.

The transition to the lowest-energy singlet excited state in octahedral nickel(II) complexes can often be observed in solution spectra and it has been extensively discussed in literatures [1–3]. Both its intensity and unusual band shape, with resolved vibronic structure at low temperature, have been analyzed with detailed theoretical models [2,9–11]. All analyses are based on model potential energy surfaces, which are also the key ingredient to the approach discussed and applied in this review. It is important to point out that established electronic structure calculations are most often based on the adiabatic approximation and are not necessarily suitable to rationalize intensities of forbidden transitions, which are dominated by effects of coupling between potential energy surfaces, emphasizing the importance of detailed analyses of experimental spectra.

2. Intensity of a spin-forbidden transition: experimental overview and qualitative application of perturbation theory

The absorption spectra of many octahedral nickel(II) complexes can easily be interpreted using the Tanabe–Sugano diagram for the d^8 electron configuration given in Fig. 1. The electronic ground state is $^3A_{2g}$, and spin-allowed transitions to three triplet excited states are expected and easily observed in solution absorption spectra. One aspect of these spectra that has been discussed in detail is the lowest-energy spin-forbidden transition. Its intensity is often high enough to be observed in many solution absorption spectra, as illustrated in literatures [1,3,5,6,12] and for three representative complexes $[Ni(imidazole)_6]^{2+}$, $[Ni(NH_3)_6]^{2+}$ and $[Ni(bipyridine)_3]^{2+}$ in Fig. 2. These three homoleptic complexes all have six nitrogen ligator atoms, but the energies of their spin-allowed bands vary significantly. The position of the weak, spin-forbidden band can be either close to the lowest-energy spin-allowed transition to the $^3T_{2g}$ final state, illustrated by the bottom two spectra in Fig. 2, or close to the $^3T_{1g}(^3F)$ band, as illustrated by the top trace in Fig. 2. For weak ligands, the transition can even be higher in energy than the $^3T_{1g}(^3F)$ band, as has been observed and studied in detail for the $[Ni(H_2O)_6]^{2+}$ complex both in solution and in the solid state and for several solid chloride and bromide host lattices doped with nickel(II) ions [4,9–18]. The Tanabe–Sugano dia-

gram in Fig. 1 illustrates that the two low-energy triplet excited states $^3T_{2g}$ and $^3T_{1g}(^3F)$ are close in energy for the range of ligand-field strengths denoted by the oval and corresponding to the complexes in Fig. 2. The third triplet excited state, $^3T_{1g}(^3P)$, has a significantly higher energy separation from $^3T_{1g}(^3F)$. This is a consequence of the interaction between the two $^3T_{1g}$ states [19]. The variation of excited state energies through relatively minor changes of the ligand sphere is attractive in order to gain insight on factors that determine intensity borrowing for forbidden transitions. It is qualitatively obvious from Fig. 2 and from the spectra in the literature that the intensity of the forbidden transition is highest when it is close in energy to the maximum of a spin-allowed band, and its intensity obviously decreases as the energy separation increases. From these qualitative observations, a simple quantitative model based on perturbation theory has been proposed for the intensity I of the spin-forbidden transition to the ^1E_g excited state [1]:

$$I = \text{const}\frac{\gamma^2}{\Delta E^2} \quad (1)$$

In this equation, γ denotes the coupling constant between one triplet excited state and the ^1E_g state. In O_h point group symmetry, this constant is equal to $\sqrt{6}\lambda$ [2] between the E_g spin-orbit levels of the ^1E_g state and those arising from the $^3T_{2g}$ and $^3T_{1g}(^3F)$ states, on the order of 700 cm^{-1} estimated from the spin-orbit coupling constant λ for the free ion, and on the order of 500–600 cm^{-1} estimated from the spin-orbit coupling constants λ, determined from magnetic susceptibility measurements and EPR experiments for octahedral complexes [3,20]. The energy difference ΔE can be roughly estimated from the band maxima of the spin-forbidden and spin-allowed absorption bands. Based on Eq. (1), the intensity I should therefore increase with the square of the coupling constant γ and decrease with the inverse square of ΔE. Experimental absorption spectra show an obvious decrease of the intensity for complexes with a large energy difference between the singlet and triplet bands, but a quantitative application of Eq. (1) is difficult, in part due to bandshapes that cannot be easily separated into spin-forbidden and spin-allowed components. It is also obvious from the spectra in Fig. 2 that the intensity of the spin-forbidden transition is impossible to determine precisely through numerical procedures. It is often observed as a shoulder on a more intense spin-allowed band. Any model to analyze the intensity of the spin-forbidden band must therefore include the bandshapes of both the allowed and forbidden transitions, as discussed in the following section.

The most detailed experimental analysis of intensity borrowing as a function of the parameter ΔE has been made through luminescence lifetime measurements at variable external pressures, mainly for a variety of doped oxide and halide lattices with octahedral sites occupied by chromium(III) ions [21]. External pressure leads to a variation of ΔE, and a model based on Eq. (1) has been successfully applied to rationalize many observations. The coupling constant γ obtained from these experiments is independent of ΔE or pressure and the inclusion of intensity borrowing from all vibronic levels has been shown to lead to a precise quantitative agreement with experimental luminescence lifetimes [21]. These experimental results and theoretical models [22,23] indicate that intensity borrowing as described by Eq. (1), i.e. from a single allowed transition, appears to be quantitatively correct if the lowest-energy electronic transition is spin-forbidden, a result that has been implicitly generalized to all spin-forbidden transitions. This review emphasizes that such a generalization can be fallible for higher-energy forbidden transitions and explores more adequate models.

3. A theoretical model for the absorption spectrum of two coupled states: the lowest-energy spin-forbidden transition and a spin-allowed band

All absorption spectra in Fig. 2 show a shoulder near the lowest-energy spin-allowed transition, traditionally assigned as the spin-forbidden $^3A_{2g} \rightarrow {}^1E_g$ band. The close proximity of the singlet and triplet excited states leads to strong mixing through spin-orbit coupling, effects that have been analyzed in detail for a number of octahedral complexes of nickel(II) [1–3,9–13]. The mixing causes an increase of the intensity and bandwidth of the spin-forbidden transition, leading to a band that is easy to detect in the spectra in Fig. 2, in contrast to all other transitions to singlet excited states, which usually are not observed in solution absorption spectra. An important consequence of the coupled excited states is the change of band shapes, which also influences the energies of the band maxima. In order to analyze these effects, a quantitative model has to be used, and calculated spectra have to be fitted to experimental data. We apply a theoretical model developed by Neuhauser et al. [7] to calculate the absorption spectrum of a forbidden spin-flip transition close in energy to an allowed interconfigurational band. This model neglects the coordinate dependence of the transition dipole and is strictly applicable only to complexes without inversion symmetry, as vibronic intensity mechanisms are not treated. It successfully reproduces the spectra of many octahedral complexes of nickel(II) [5,6,13] and chromium(III) [13] where coupled electronic states of different multiplicity occur, indicating that the assumption of an allowed transition does not lead to significant discrepancies between experimental and calculated spectra. In the following, we review the results obtained from the application of this model to six-coordinate nickel(II) complexes with and without inversion symmetry.

Fig. 3 illustrates the model. The potential energy curves for the $^3A_{2g}$ ground state as well as the ^1E_g and a single $^3\Gamma$ excited states are given by the solid traces in Fig. 3, which can be calculated from the harmonic approximation and ground-state Raman frequencies. Identical frequencies define all harmonic potential energy curves for the electronic states in Fig. 3. We use the same symbols for all quantities as given in the original publication of this model [7]. The energy minimum of the ground-state potential energy curve corresponds to the equilibrium geometry. As no metal–ligand bonding changes occur in the singlet excited state, its minimum is placed at the same position as the ground state minimum along the normal coordinate in Fig. 3. The minimum for the $^3\Gamma$ excited state is offset by ΔQ along one or several normal coordinates. In the absence of coupling, the band max-

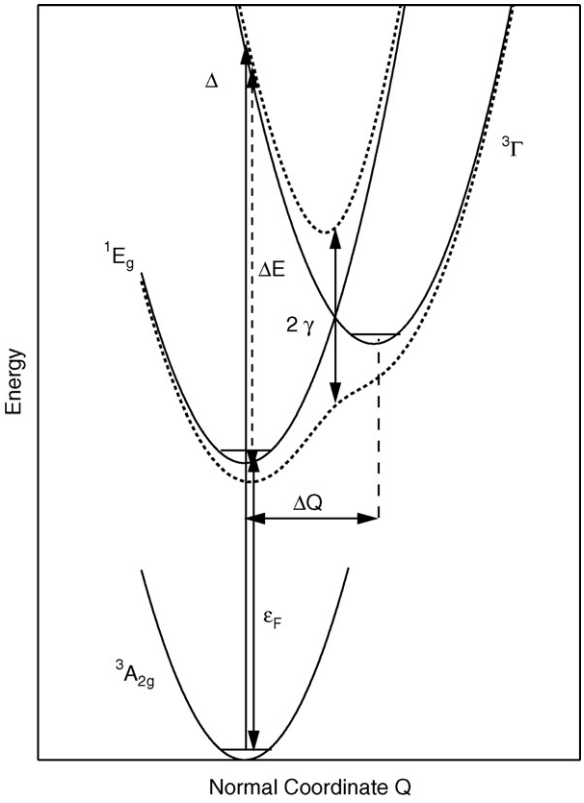

Fig. 3. Model for an absorption spectrum involving the lowest-energy singlet excited state (^1E_g) and one triplet excited state ($^3\Gamma$) of octahedral nickel(II) complexes. Diabatic and adiabatic potential energy surfaces are given as solid and dotted traces, respectively and parameters used to calculate spectra are defined. Of particular importance are the coupling constant γ and the energy difference ΔE between the vertical transitions to the diabatic potential energy curves for the singlet and triplet excited states.

imum of the triplet band is given by the parameter Δ, and the forbidden transition occurs at energy ε_F. The energy difference ΔE in Eq. (1) is calculated as the difference between ε_F and Δ. The solid-line diabatic potential energy curves describe the singlet and triplet excited states in the absence of coupling, i.e. for a coupling constant γ of zero. Nonzero values for γ lead to the adiabatic potential energy surfaces shown as dotted curves in Fig. 3, different from the harmonic diabatic curves. Both sets of curves are necessary to calculate the absorption band system arising from transitions to these coupled excited states. The Hamiltonian for the two excited states described by the coupled potential energy surfaces is given by [7]:

$$H = \frac{p^2}{2M}\begin{bmatrix} 1 & 0 \\ 0 & 1 \end{bmatrix} + \begin{bmatrix} \frac{1}{2}M\omega_0^2 x^2 + \varepsilon_F & \gamma \\ \gamma & \frac{1}{2}M\omega_0^2(x - x_A)^2 + \varepsilon_F - \Delta E \end{bmatrix} \quad (2)$$

Analytical and numerical solutions for the absorption spectrum resulting from transitions to these two coupled excited states have been published and discussed [7,13]. The calculated spectrum involving the coupled states is given by:

$$\sigma(\omega) = \frac{1}{2\pi}\int_{-\infty}^{\infty} \left\langle \Psi_0 | e^{-i(H-\omega)t - \Gamma|t|} | \Psi_0 \right\rangle dt = \frac{1}{\pi} \mathrm{lm} \left\langle \Psi_0 | (H - \omega - i\Gamma)^{-1} | \Psi_0 \right\rangle, \quad (3)$$

The absorption spectra in Fig. 2 do not allow an experimental determination of all triplet excited levels arising from $^3T_{2g}$ or $^3T_{1g}$ split by deviations from octahedral symmetry and spin-orbit coupling. We describe the band shape for the allowed transition to the triplet excited state in the absence of coupling to the singlet excited state by a Lorentz profile with a width of $\sqrt{\omega_0\lambda}$ [7]. With this simplification, which also makes it unnecessary to specify individual normal coordinates and offsets ΔQ, an analytical equation for the absorption spectrum is obtained [7]:

$$\sigma(\omega) = -\frac{1}{\pi}\mathrm{lm}\left(\frac{\beta}{1 - \gamma^2\alpha\beta}\right) \quad (4)$$

where α and β are defined as:

$$\alpha = \frac{1}{\omega - \varepsilon_F + i\Gamma}, \qquad \beta = \frac{1}{\omega - \Delta + i\sqrt{\omega_0\lambda}} \quad (5)$$

Γ in Eqs. (3) and (5) denotes the vibronic line width of each transition. This model has been applied in the literature with two quantitative goals. The original reason for its development and the first scientific goal was to explore interference effects arising from the coupled final states of a forbidden and a single allowed transition in absorption spectra of molecules. Interference dips occur in such spectra, and their formal relationship to Fano antiresonances observed in atomic spectroscopy was derived [7]. Second, the model leads to precise energies ε_F of the forbidden transition in the absence of coupling. These values have been discussed in terms of interelectronic repulsion effects and are of particular relevance for complexes with a mixed ligand sphere, where empirical correlations such as the nephelauxetic series [24] cannot be applied in a straightforward way and where the energies of the singlet excited state have to be known precisely [5,6]. In this review, we focus on a third aspect not discussed before: the intensity of the spin-forbidden transition, in particular its variation as a function of the coupling constant γ and the energy difference ΔE in Eq. (1). We will compare the intensities calculated for a spin-forbidden transition from the model described by Eq. (4) and compare to the expectation from Eq. (1).

A series of calculated spectra used to determine the intensity of the forbidden transition is shown in Fig. 4. All spectra show a weak spin forbidden band at an energy defined by the ε_F value of 8000 cm^{-1} and an intense spin-allowed band with its maximum at an energy Δ higher than 10,000 cm^{-1}. In Fig. 4a, the energy Δ is varied, showing the effect of ΔE on the intensity of the forbidden transition. It is qualitatively obvious that the spin-forbidden band is most intense in the spectrum with the smallest value of ΔE. Numerical integration of the spin-forbidden band leads to the intensity decrease with increasing

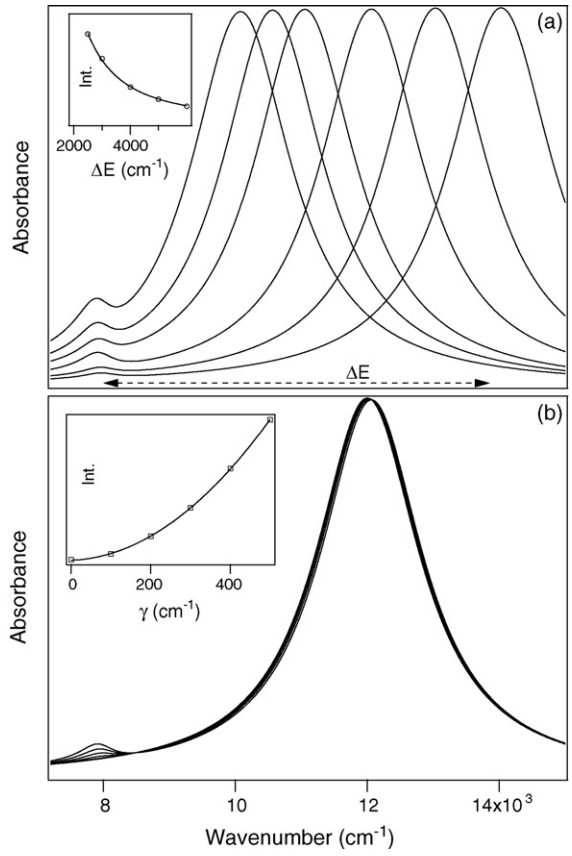

Fig. 4. Calculated absorption spectra obtained with Eq. (4) for the transition to the coupled singlet and triplet excited states illustrated in Fig. 3. The energy ε_F of the singlet excited state is set to 8000 cm^{-1} for all calculations. (a) Variation of the energy difference ΔE between the singlet and triplet excited states. The inset shows the intensity of the forbidden transition as a function of ΔE with a fit to Eq. (1). (b) Variation of the coupling constant γ. The inset shows the intensity of the forbidden transition as a function of γ with a fit to Eq. (1).

ΔE shown in the inset to Fig. 4a. The trace in the inset is a fit to Eq. (1) with a constant value of γ, indicating that the model defined by Eq. (4) is in quantitative agreement with Eq. (1). Fig. 4b shows calculated spectra for different values of the coupling constant γ. The intensity of the spin-forbidden transition increases with γ, and the intensity obtained by numerical integration is shown in the inset to Fig. 4b. The solid trace again is a fit to Eq. (1) with a constant value of ΔE, illustrating that the calculated intensity increases as described by Eq. (1). Fig. 4 confirms that absorption spectra calculated with Eq. (4) for different values of γ and ΔE lead to the intensity variation of the spin-forbidden transition expected from Eq. (1), determined by intensity-borrowing through spin-orbit coupling with a single spin-allowed transition. Any increase of γ or decrease of ΔE leads to more triplet character mixed into the wavefunction of the ^1E_g state and to an increase of the intensity for the spin-forbidden transition.

A model based on the full set of coupled potential energy curves shown in Fig. 3 has to be applied for a precise analysis of the absorption spectra in Fig. 2, as shown in the following section for a number of nickel(II) complexes. In order to analyze experimental spectra with this model, as many parameters as possible were set to experimental quantities. Vibrational frequencies ω_0 were held constant at values observed in the Raman spectra and initial values for Δ and ε_F were estimated from the experimental absorption spectra. The coupling constant y was limited to values lower than 1000 cm^{-1}, corresponding to the order of magnitude of the spin-orbit coupling constant for nickel(II). Only λ, a factor contributing to the width of the spin-allowed absorption band, and Γ, whose role in Eq. (4) is to define the width of the spin-forbidden band, were treated as freely adjustable parameters without numerical constraints. The most important parameter values obtained from the fits are the coupling constants γ and energy differences ΔE, calculated as $\varepsilon_F - \Delta$, leading to a set of data points ideally suited to test the assumptions underlying Eqs. (1) and (4).

4. Analysis of the room-temperature absorption band system in solution with the model based on two coupled states

The model defined by Eq. (4) and illustrated in Figs. 3 and 4 has been applied in the literature to the solution absorption spectra of eight octahedral nickel(II) complexes [5,6,13]. Fig. 5 shows the fit of Eq. (4) to the absorption spectra of $[Ni(imidazole)_6]^{2+}$, $[Ni(NH_3)_6]^{2+}$ and $[Ni(bipyridine)3]^{2+}$ complexes, whose full d–d spectra are shown in Fig. 2 and illustrates the excellent agreement between fits and experimental spectra. The bandshapes including one spin-forbidden and one spin-allowed transition are well reproduced by the fits, demonstrating that the model described in the preceding section provides an easy quantitative way to calculate many different spectra with weak or intense spin-forbidden bands. For the $[Ni(H_2O)_6]^{2+}$ complex, a detailed comparison between parameter values obtained with Eq. (4) and those from numerical models explicitly describing the normal coordinate and potential energy surfaces in Fig. 3 has been made and it has been shown that the parameters resulting from Eq. (4) are reliable [13]. All parameters obtained from the fits are summarized in Table 1 for the complexes used in this review.

The sensitivity to values of the coupling constant γ is qualitatively illustrated for the spectrum of $[Ni(NH_3)_6]^{2+}$ in Fig. 5b. The best fit is superimposed to the experimental spectrum and leads to a coupling constant y of 305 cm^{-1}, lower by almost a factor of two than the value on the order of 500–600 cm^{-1} estimated from the ligand-field matrix element. The solid trace offset from the experimental spectrum in Fig. 5b is a fit where the coupling constant γ was held fixed at 500 cm^{-1}. It is obvious that this calculated spectrum is in marked disagreement with the experimental absorption band system, illustrating the narrow limits imposed on parameter ranges by the fit of Eq. (4). Other parameter values have only a small influence on the coupling constant γ, as illustrated for the [Ni(tris(3,5-dimethylpyrazolyl)methane)$(NO_3)_2$] complex [6] where two different vibrational frequencies ω_0, corresponding to different Raman transitions, lead to γ values that vary by less than 10%, as documented in Table 1. This table summarizes all parameter values obtained from the analysis of spectra with Eq. (4). In addition to results from room-temperature solution spectra, we have included values for two

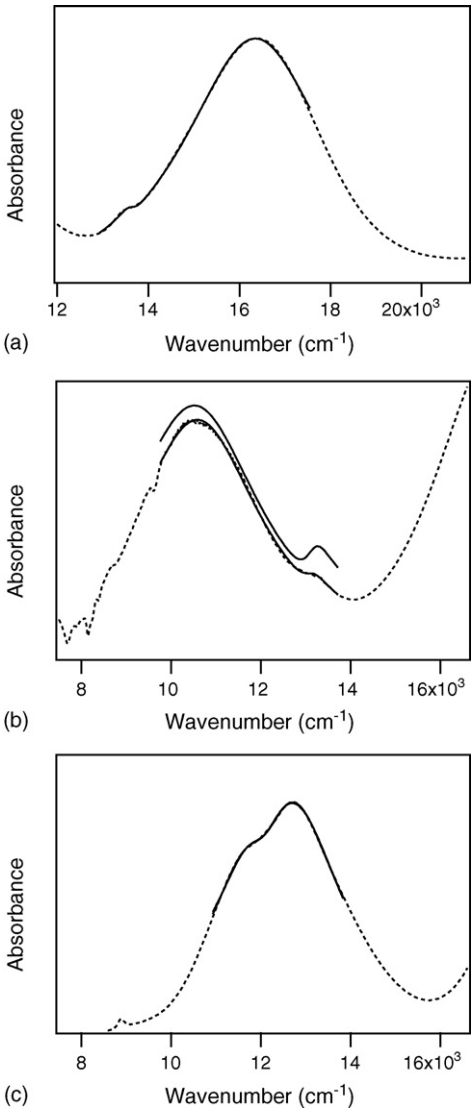

Fig. 5. Comparison of experimental and calculated absorption spectra, shown as dotted and solid lines, respectively. Calculated spectra are shown for the wavenumber range used in the least-squares fit. All parameters obtained are given in Table 1. (a) $[Ni(imidazole)_6]^{2+}$, (b) $[Ni(NH_3)_6]^{2+}$ including a spectrum resulting form a least-squares fit where the coupling constant γ was held at 500 cm^{-1}, offset along the ordinate for clarity, and (c) $[Ni(bpy)_3]^{2+}$.

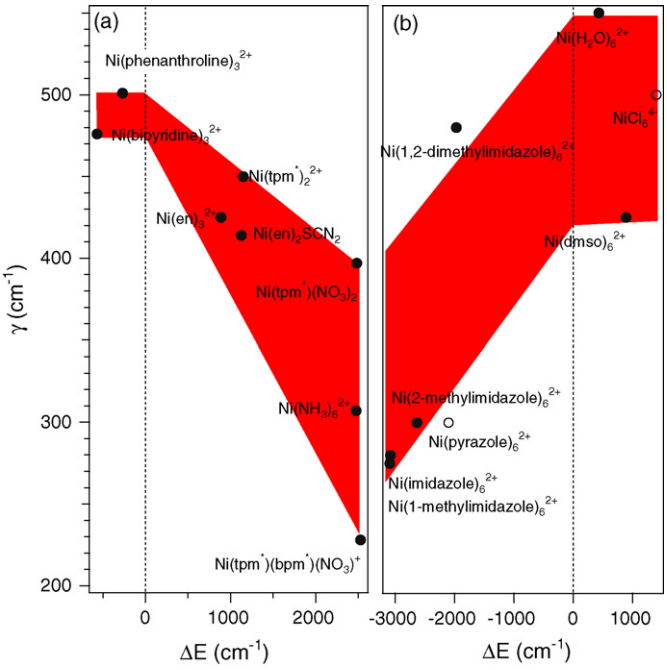

Fig. 6. Comparison of γ and ΔE values obtained from the fit of Eq. (4) to experimental absorption spectra. (a) The $^3T_{2g}$ excited state is closest in energy to the ^1E_g excited state. The dotted vertical line denotes the energy of the $^3T_{2g}$ excited state, as given by the parameter Δ in Table 1. (b) Comparison of γ and ΔE for complexes with the $^3T_{1g}(^3F)$ excited state closest in energy to ^1E_g. The dotted vertical line denotes the energy of the $^3T_{1g}(^3F)$ excited state, as given by the parameter Δ in Table 1. The two open symbols denote results from low-temperature single-crystal spectra. Ligand abbreviations: en: ethylenediamine, tpm^*: (tris(3,5-dimethylpyrazolyl)methane), dmso: dimethylsulfoxide, bpm^*: bis(3,5-dimethylpyrazolyl)methane.

low-temperature single-crystal spectra reported in the literature for $[Ni(pyrazole)_6](NO_3)_2$ [25] and for $CsCdCl_3$ doped with nickel(II) ions, leading to octahedral $[NiCl_6]^{4-}$ chromophores [26]. Both spectra show a weak, unresolved band for the lowest-energy spin-forbidden transition phenomenologically similar to the solution spectra, and their spectra are therefore well suited for an analysis with Eq. (4).

One striking aspect of the parameter values obtained from fits of Eq. (4) and presented in Table 1 is illustrated in Fig. 6. Surprisingly, the values of the coupling constants γ and energy differences ΔE show a distinct correlation. Fig. 6a summarizes the values for complexes where the ^1E_g state is closer in energy to the $^3T_{2g}$ state than to the $^3T_{1g}(^3F)$ state. The fit of Eq. (4) was therefore made to the $^3T_{2g}$, ^1E_g band system of the experimental spectrum. The dotted vertical line denotes the band maximum Δ of the $^3T_{2g}$ transition and is the point of reference from which ΔE values are plotted in Fig. 6a. The highest values for γ are obtained for the smallest absolute values of ΔE, and a distinct decrease of γ is observed as ΔE increases and the transition to the ^1E_g state occurs in the region of low absorbance between the $^3T_{2g}$ and $^3T_{1g}(^3F)$ bands. To the low-energy side of the $^3T_{2g}$ band, corresponding to negative values of ΔE in Fig. 6a, the coupling constant γ appears to be constant as the spin-forbidden band is located lower in energy than the $^3T_{2g}$ band. This region corresponds to the complexes with the strongest ligands $[Ni(bipyridine)_3]^{2+}$ and $[Ni(phenanthroline)_3]^{2+}$. It is interesting to note that an exchange of the numerical values of ε_F and Δ does not lead to a good agreement with the experimental spectrum, showing that Eq. (4) can even be used to determine the energy order of the two coupled excited states via the band-shape of the absorption spectrum. Fig. 6b summarizes the γ and ΔE values obtained for complexes where the ^1E_g band is closer to the band maximum A of the $^3T_{1g}(^3F)$ transition, defined by the dotted vertical line analogous to Fig. 6a. Again, the highest coupling constants γ are observed for the smallest absolute values of ΔE. A strong and distinct decrease is observed on the low-energy side of the vertical line, indicating that γ values go through a minimum in the region between the two spin-allowed absorption bands. For this intermediate region, the choice of triplet band to include for the fit of Eq. (4) often appears somewhat arbitrary,

Table 1
Parameter values obtained from the fit of Eq. (4) to experimental absorption spectra

Complex	ε_F	Δ	ΔE[a]	γ	ω_0	λ	Γ
Ni(bipyridine)$_3^{2+}$	11,989	12,473	−484	338	345	7,901	513
Ni(phenanthroline)$_3^{2+}$[b]	12,006	12,276	−270	545	450	3,022	796
Ni(ethylenediamine)$_3^{2+}$[b]	12,326	11,552	774	530	446	5,206	900
Ni(en)$_2$(SCN)$_2$	12,659	11,444	1215	414	431	6,868	883
Ni(tpm*)$_2^{2+}$[c]	12,923	11,773	1150	450	423	7,463	500
Ni(tpm*)(NO$_3$)$_2$[c]	12,854	10,370	2214	397	222	9,760	274
Ni(tpm*)(NO$_3$)$_2$[c]	12,873	10,389	2484	436	577	3,760	274
Ni(NH$_3$)$_6^{2+}$	13,079	10,620	2459	305	344	9,012	303
Ni(tpm*)(bpm*)(NO)$_3$[c]	12,994	10,465	2529	228	416	7,454	188
Ni(imidazole)$_6^{2+}$	13,626	16,339	−2713	186	345	11,566	194
Ni(l-Meim)$_6^{2+}$	13,148	16,261	−3113	275	398	10,628	313
Ni(2-Meim)$_6^{2+}$	13,165	15,801	−2636	300	329	8,547	400
Ni(pyrazole)$_6^{2+}$[d]	13,300	11,200	−2100	300	350	3,600	250
Ni(l,2-DiMeim)$_6^{2+}$	13,380	15,406	−2026	500	535	10,321	786
Ni(H$_2$O)$_6^{2+}$[e]	14,757	14,325	432	550	380	7,620	630
Ni(dmso)$_6^{2+}$[c]	14,027	13,138	889	425	390	6,770	556
NiCl$_6^{4-}$[f]	12,400	11,000	1400	500	300	1,200	300

Example fits are shown in Fig. 5. Symbols are defined in Section 3 and Fig. 3. All values are given in cm^{-1} units. The values for γ and ΔE are shown in Fig. 6.
[a] $\Delta E = \varepsilon_F - \Delta$.
[b] Ref. [5].
[c] Ref. [6], tpm*: tris(3,5-dimethylpyrazolyl)methane, bpm*: bis(3,5-dimethylpyrazolyl)methane.
[d] Solid-state spectrum from Ref. [25].
[e] Ref. [13].
[f] Solid-state spectrum from Ref. [26].

as the energy differences between the spin-forbidden band and either band maximum of the neighboring spin-allowed bands are comparable.

The overall variation of γ by approximately a factor of two and leading to a "V-shape" systematic variation with ΔE as shown by the shaded areas in Fig. 6 is unexpected and not physically justified: experimental spin-orbit coupling constants do not vary by this much for octahedral nickel(II) complexes and they do not depend on energy differences between singlet and triplet excited states [3,20]. The observations in Fig. 6 indicate that the model described by Eqs. (1) and (4) is incomplete and that additional effects outside the scope of Eqs. (1) and (4) are leading to unreasonably low values of γ if these equations are used to calculate spectra. The most obvious additional effect is the influence of the second spin-allowed transition. Any calculated spectra obtained with Eq. (4) neglect all additional triplet excited states, but the spectra in Fig. 2 show that the spin-forbidden absorption band is often relatively close to two spin-allowed bands, in particular for complexes such as [Ni(imidazole)$_6$]$^{2+}$, shown in Fig. 5a.

Different substituents of the imidazole ligand have a subtle influence on the spin-allowed transitions and show markedly different γ values, as illustrated in Fig. 6b, again confirming the apparent correlation of γ and ΔE. It is obvious that a sum of two spectra calculated with Eq. (4) does not solve the problem of the low value obtained for the coupling constant γ: adding two calculated spectra would further increase the intensity of the forbidden transition and would force any fit procedure to produce an even lower numerical value for the coupling constant γ. All allowed transitions have to be considered simultaneously, and this can no longer be achieved by the analytical equation (4).

5. The effect of two allowed bands on the intensity of the lowest-energy spin-forbidden transition

In this section, we present calculated absorption spectra obtained from a model involving two spin-allowed transitions and three coupled excited states, the $^3T_{2g}$, ^1E_g and $^3T_{1g}(^3F)$ states in Fig. 1. As stated before, the coupling constant γ is expected to be on the order of 500–600 cm^{-1} in many homoleptic complexes of nickel(II). Eq. (4) cannot be generalized to two allowed transitions, and therefore numerical calculations are required [12,23,27–31]. Three harmonic potential energy surfaces along a single normal coordinate are used to represent the three excited states, a straightforward generalization of the model shown in Fig. 3 for which we again neglect the coordinate dependence of the transition dipole. The coupling constants γ are held constant at a value of 500 cm^{-1} for all calculations. The resulting spectra are shown in Fig. 7. Solid traces denote calculated spectra for three coupled states, dotted traces those for the same three excited states, but with nonzero coupling only between ^1E_g and one triplet excited state, i.e. calculations corresponding to those obtained with Eq. (4) and shown in Fig. 5. For the dotted spectra (a) and (b), nonzero coupling is chosen with the higher-energy triplet excited state, for the dotted spectra (c–h) coupling occurs with the lower-energy triplet excited state. It is obvious from all spectra in Fig. 7 that the forbidden transition is most intense if it is close in energy to an allowed band, as observed in the experimental absorption spectra. The most interesting situation occurs for the forbidden transition at energies between the two allowed bands, illustrated by the solid and dotted traces (c). The inset to Fig. 7 shows an enlarged view of this region, and it is obvious that the dotted spectrum,

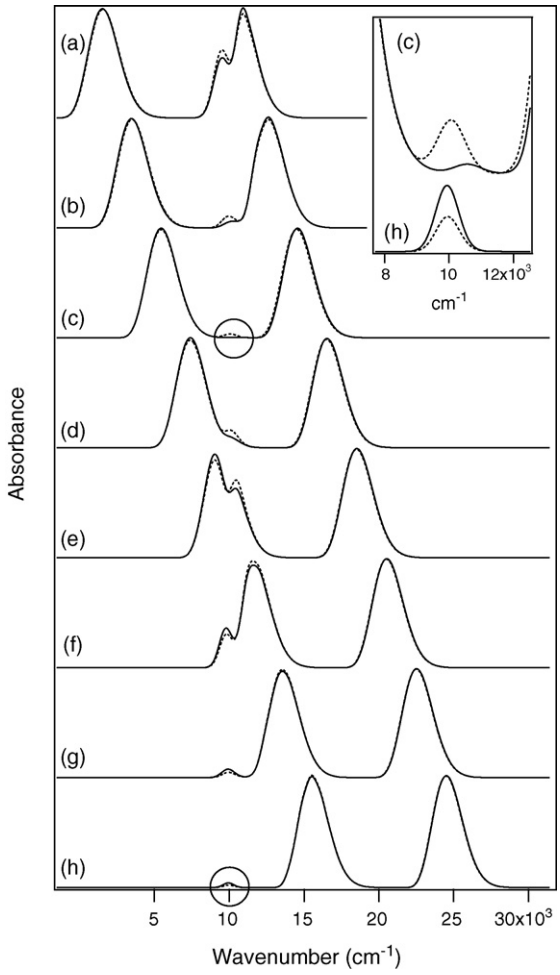

Fig. 7. Calculated absorption spectra resulting from two triplet excited states coupled to a singlet state. Solid traces: two triplet states coupled to the lowest-energy singlet excited state. Dotted traces: one triplet state coupled to the lowest-energy singlet state. Spectra (a) and (b): the higher energy triplet state is coupled to the singlet, spectra (c)–(h): the lower energy triplet state is coupled to the singlet. Inset: enlarged view of the spin-forbidden transition for the two regions denoted by circles in the main figure for spectra (c) and (h).

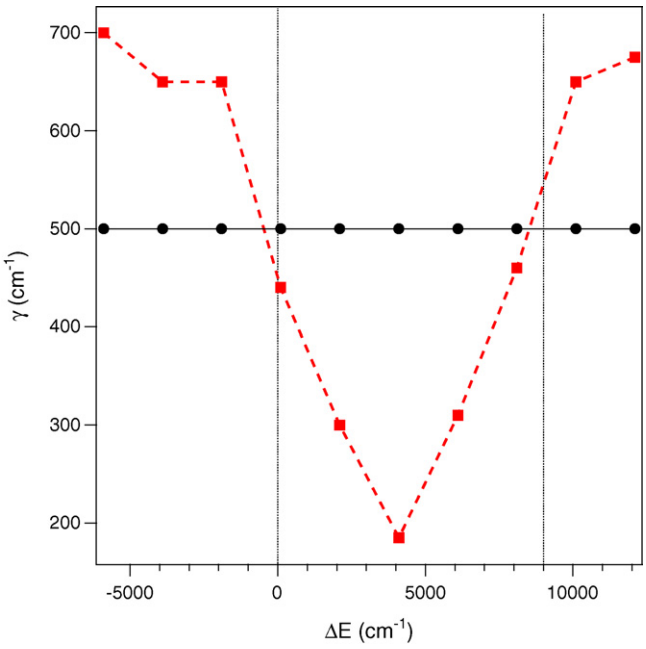

Fig. 8. Comparison of coupling constants γ used to calculate the spectra shown as solid lines in Fig. 7 (circles connected by solid lines) and coupling constants used to reproduce the intensity of the forbidden band with a model based on only one allowed transition (squares connected by dotted lines). The two vertical dotted lines denote the energies of the maxima of the two spin-allowed transitions with energy differences ΔE given relative to the lower energy spin-allowed band maximum in Fig. 7.

obtained with nonzero coupling between the singlet and a single triplet state, leads to a significantly more intense forbidden transition than the solid spectrum obtained with nonzero coupling matrix elements between ^1E_g and both triplet excited states. This observation qualitatively explains the surprising decrease of the coupling constants γ obtained in the preceding section and shown in Fig. 6 for complexes with the forbidden transition located at energies between the two allowed bands. The two spin-allowed transitions lead to destructive interference and a lower intensity for the forbidden transition, despite an undeniably higher triplet character of the ^1E_g wavefunction due to the two nonzero coupling constants.

For complexes with a spin-forbidden transition lower in energy than both spin allowed bands, corresponding to spectra (h) in Fig. 7, the enlarged view in the inset shows a much smaller intensity difference between the intensities given as dotted and solid traces. In contrast to the decrease of the intensity discussed above, a small increase of the intensity is observed in this energy range, corresponding to a constructive interference. This aspect of the model calculations underlines that the situation explored by pressure-dependent luminescence spectroscopy of chromium(III) complexes (variation of ΔE) [21] and theoretical studies on complexes with a spin-forbidden lowest-energy excited state [22] are a special category, and the calculated spectra in Fig. 7 confirm that for this case a model limited to two coupled excited states is appropriate.

The intensity of the spin-forbidden band calculated with three coupled excited states and shown as solid lines in Fig. 7 can be reproduced with a model involving only two coupled excited states. The coupling constant γ has to be adjusted, and the resulting values are shown in Fig. 8. A "V-shape" variation with a minimal value for γ between the two allowed transitions, qualitatively similar to Fig. 6, is obtained from this adjustment, illustrating the limits of the model based on two coupled excited states. At the lowest ΔE values, the value of γ has to be increased in order to reproduce the spectrum shown as a solid line in Fig. 7, confirming the constructive interference between the two allowed transitions and the forbidden band for situations where the lowest-energy transition is forbidden.

Spin-forbidden transitions located in energy between allowed transitions from which they can borrow intensity are therefore not well characterized by models such as those defined by Eqs. (1) and (4) that take into account only a single coupling matrix element. The two single-crystal absorption spectra whose parameters are included in Fig. 6 illustrate that this interference effect is significant for spin-forbidden bands located between the two lowest-energy spin-allowed transitions, the area outlined by the oval in Fig. 1. The effect on bands located between the

two higher-energy $^3T_{1g}$ excited states is expected to be weaker because of the larger energy separation of these two states, as confirmed on the right-hand side of Fig. 6b by the slower decrease of y with increasing ΔE. Qualitatively, the spectra and calculations for spin-forbidden transitions lower in energy than all spin-allowed bands and for spin-forbidden transitions at energies between spin-allowed bands separated by a large energy difference show a small variation of γ, and models based on Eq. (4) are appropriate. The calculated spectra in Fig. 7 show that the intensity of a forbidden band does not simply increase with each additional coupling pathway to an allowed transition and they qualitatively rationalize the origin of the surprising variation of the coupling constant γ with the energy separation ΔE presented in Fig. 6. We are currently exploring detailed spectra and model calculations that quantitatively reproduce the observed intensity variations. Such effects are also likely to influence transition intensities between excited states, processes of crucial importance in upconversion materials, where intensities and vibronic patterns different from the expectations based on electronic configurations are common [4,26,32].

6. The lowest-energy spin-forbidden transition in low-temperature absorption spectra of crystalline $MgBr_2:Ni^{2+}$ and $CsMgBr_3:Ni^{2+}$

In order to further examine the spectroscopic manifestations of multiple coupled excited states on the lowest-energy spin-forbidden band, it is obviously attractive to analyze single-crystal absorption spectra at low temperature. Such spectra often show resolved vibronic structure, providing direct information on excited-state vibrational frequencies and, in the case of several octahedral nickel(II) complexes, information on coupled excited states [9,11]. In this section, we analyze the particularly well resolved spectrum of MgBr2:Ni^{2+} in the region of the lowest energy spin-forbidden transition to the ^1E_g state and compare it to the similar, but somewhat less resolved spectrum of $CsMgBr_3:Ni^{2+}$. Progression intervals in absorption spectra often allow a direct experimental determination of excited-state vibrational frequencies for many transition metal complexes. Successful quantitative analyses with harmonic potential energy surfaces have been carried out and metal–ligand bond-length changes and other excited-state distortions have been reported for a large number of transition metal complexes [28,30].

In special situations, interactions between electronic states have been shown to influence the observed energy intervals within resolved progressions. The best known nickel(II) complex illustrating this behavior is $[Ni(H_2O)_6]^{2+}$, whose "red band", corresponds to the spin-forbidden transition to the ^1E_g excited state in proximity to the spin-allowed band with the $^3T_{1g}(^3F)$ final state [2,9–12,33,34]. This band system shows a prominent series of four resolved peaks in low-temperature single crystal spectra. Their average energy separation is on the order of 490 cm^{-1}, larger than the Raman-active ground-state metal–ligand stretching frequency of approximately 400 cm^{-1} and has been shown to be determined by coupling between the E_g spin-orbit levels arising from the ^1E_g and $^3T_{1g}(^3F)$ states [9]. The low-temperature single-crystal spectra can be quantitatively analyzed with a model involving these two coupled excited states as shown in Fig. 3 [11].

Crystalline nickel(II) halides and halide host lattices doped with nickel(II) ions in approximately octahedral coordination geometry show absorption band systems with qualitative similarities to $[Ni(H_2O)_6]^{2+}$ [11]. Several nickel(II) chlorides show a $^3T_{1g}(^3F)$, ^1E_g band system with a well-resolved, short progression with three to four members on the high-energy side of the band. The progression intervals of approximately 300 and 330 cm^{-1} are higher than the totally symmetric stretching frequency on the order of 260 cm^{-1} for $CsNiCl_3$ ($CsMgCl_3:Ni^{2+}$) and $NiCl_2$ [4,14–16,35]. The richest vibronic structure is observed for octahedral complexes with bromide ligands, compounds, which often show well-resolved absorption spectra [4,14–16]. Their low-frequency metal–ligand vibrations lead to long progressions, allowing a detailed comparison of progression intervals and intensity distributions with those obtained from model calculations based on potential energy curves as shown in Fig. 3. Fig. 9a illustrates the low-temperature, single-crystal spectrum of $[NiBr_6]^{4-}$ molecular units in $MgBr_2:Ni^{2+}$ [4]. Similar spectra are observed for the nickel(II) doped bromide host lattice $CsMgBr_3$ [4,14,15] and its lowest-energy spin-

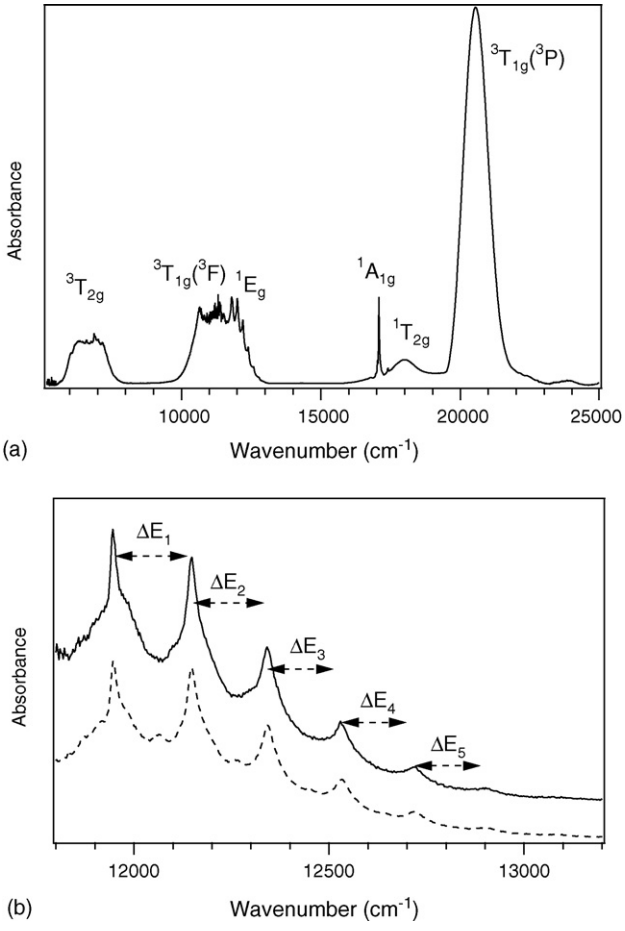

Fig. 9. (a) Overall absorption spectrum of $MgBr_2:Ni^{2+}$. Assignments in O_h point group symmetry for triplet excited states and singlet states are given and (b) detailed absorption spectra of $MgBr_2:Ni^{2+}$ in the region of the lowest-energy singlet transition in σ and π polarization are shown as solid and dotted traces, respectively. Energy intervals ΔE_i are given in Table 2.

Table 2
Experimental band maxima and energy differences ΔE_i within the prominent progression for the spectra of $MgBr_2:Ni^{2+}$ and $CsMgBr_3:Ni^{2+}$ shown in Figs. 9b and 11

Maxima E_i	$MgBr_2:Ni^{2+}$			$CsMgBr_3:Ni^{2+}$		
E_1	11,802			13,597		
E_2	12,005			13,791		
E_3	12,200			13,984		
E_4	12,389			14,178		
E_5	12,574			14,376		
E_6	12,758			14,572		
Differences ΔE_i	Experimental	Calculated D_{3d}	Calculated O_h	Experimental	Calculated D_{3d}	Calculated O_h
ΔE_1	203	199	215	194	199	212
ΔE_2	195	197	210	193	198	209
ΔE_3	189	195	207	194	197	206
ΔE_4	185	193	203	198	197	205
ΔE_5	184	192	201	196	195	202

Energy differences ΔE_i obtained from the calculated spectra in Fig. 11 are included for comparison. All values are given in cm^{-1} units. Experimental values are estimated to be precise to within 3 cm^{-1}.

forbidden band will also be analyzed for comparison. The point group symmetry at the magnesium(II) sites is D_{3d} for both lattices, but the site structure is different, with the coordination geometry for nickel(II) in $MgBr_2$ corresponding to a trigonally compressed octahedron [36] in contrast to $CsMgBr_3$, where the metal site is a trigonally elongated octahedron [15,37]. The overall spectrum in Fig. 9a is easily rationalized in terms of an approximate O_h point group symmetry. The expected three spin-allowed transitions to triplet excited states are observed at much lower energies than those for the complexes with nitrogen donor ligands in Fig. 2, as expected from the spectrochemical series. Polarized spectra do not show distinct dichroisms of any spin-allowed band and no clearly separated band maxima due to the trigonal site symmetry are apparent in the overall spectra. The region of interest for a comparison with model calculations is between 11,500 and 13,000 cm^{-1}, where a prominent progression with at least six members is observed as part of the transitions to the $^3T_{1g}(^3F)$, ^1E_g excited states, illustrated in detail in Fig. 9b. Energies of the maxima and energy differences ΔE_i illustrated in Fig. 9b are given in Table 2 for both the doped $MgBr_2$ and $CsMgBr_3$ host lattices The average energy separations are 190 and 194 cm^{-1} for $MgBr_2:Ni^{2+}$ and $CsMgBr_3:Ni^{2+}$, respectively. A very similar average interval of 202 cm^{-1} has been reported for $NiBr_2$ [16] again significantly higher than the totally symmetric Raman frequencies reported as 168 cm^{-1} [16] and 170 cm^{-1} [35]. This comparison confirms that the observed progression is qualitatively identical to those analyzed before for crystalline $[Ni(H_2O)_6]^{2+}$ and $[NiCl_6]^{4-}$ [11].

It is interesting to note that the energy differences observed in Fig. 9b for $MgBr_2:Ni^{2+}$ decrease along the progression from 201 to 183 cm^{-1}. To the best of our knowledge, this is the only clear-cut documented example for energy differences that are not constant in resolved progressions for nickel(II) complexes. It is possible to observe this effect because of the low vibrational frequencies, leading to a larger number of peaks in a progression in bromide lattices, and because of the exceptional resolution obtained in the absorption spectra of $MgBr_2:Ni^{2+}$ The analysis of the spectrum presented here is focused on the well-resolved progression shown in Fig. 9b. In order to analyze the spectrum in Fig. 9b, we use the Hamiltonian given in Eq. (2) to define the coupled potential energy surfaces [29].

A model for octahedral point group symmetry is illustrated in Fig. 10a. Spin-orbit coupling mixes the two E_g levels arising from the ^1E_g and $^3T_{1g}$ states, leading to the adiabatic potential energy curves shown as dotted lines in Fig. 10a. The harmonic (diabatic) potential curves correspond to the diagonal elements of the right-hand side of Eq. (2), and the non-harmonic (adiabatic) curves correspond to the eigenvalues of Eq. (2) [29]. Figs. 3 and 10 show these potential energy curves as dotted and solid lines, respectively, along the single normal coordinate Q. The harmonic potential energy curves are defined by the frequency of the totally symmetric breathing mode, reported for the ground state of the isostructural $NiBr_2$ to be 170 cm^{-1} [35]. We use this value for the singlet excited state, the upper diagonal element in the right-hand side of Eq. (2). The minimum for the diabatic singlet excited state curve is at the origin of the Q axis, at the same position as the ground state minimum. The energy difference between the ground and singlet excited state potential energy minima is ε_F, determined from the lowest-energy maximum of the o polarized spectrum in Fig. 9b. The diabatic potential energy curve for the triplet excited state, given by the lower diagonal element in Eq. (2), has its minimum offset from the singlet excited state both along the normal coordinate axis and along the energy axis by ΔQ and ΔE, respectively. Coupling between these two states is given by the constant y, the off-diagonal element in the right-hand side of Eq. (2). All calculations presented in the following correspond to a situation where the singlet band gains its entire intensity from the triplet transition. Potential energy curves for the other spin-orbit levels arising from $^3T_{1g}(^3F)$ are included in Fig. 10a, but they do not couple with the singlet excited state. Theoretical models involving the two coupled potential energy surfaces have been shown to reproduce both the observed energy intervals and intensities of these bands for the spectra of $[Ni(H_2O)6]^{2+}$ and $[NiCl_6]^{4-}$ [11] forming progressions similar to the example shown in Fig. 9b. Qualitatively, the higher-energy adiabatic E_g potential energy

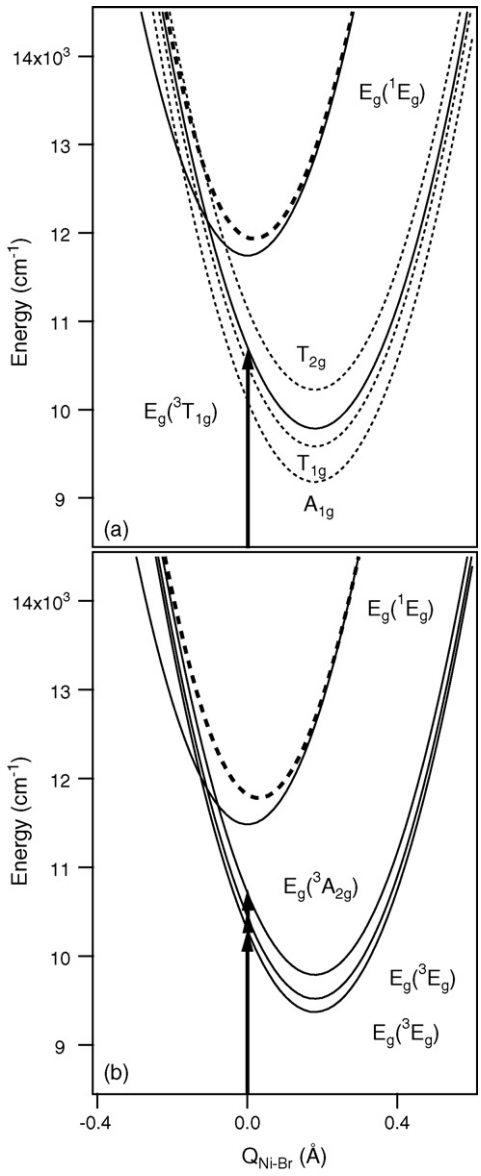

Fig. 10. Potential energy surfaces used to calculate absorption spectra: (a) O_h point group symmetry and (b) D_{3d} point group symmetry.

surface obtained including spin-orbit coupling is easily seen to be narrower than the diabatic harmonic potential energy surface describing this state without spin-orbit coupling, leading to a higher energy separation of vibronic levels and non-constant intervals between vibronic band maxima forming the progression in Fig. 9b. For the analysis of the series of peaks shown in Fig. 9b it is sufficient to consider only the two E_g states, as the other spin-orbit levels of $^3T_{1g}$ do not have the appropriate symmetry and E_g levels arising from other excited states are too far removed in energy to have a significant influence on the spectrum.

Spectra are calculated from the potential energy surfaces defined in Eq. (2) and shown in Fig. 10 using the time-dependent theory of spectroscopy [12,23,27–31]. The spectrum calculated with this approach consists of two distinct bands: at low energy, a band with closely spaced vibronic transitions and at higher

Table 3
Angular overlap parameters for $[NiBr_6]^{4-}$ determined from the absorption spectra of $MgBr_2$:Ni^{2+} and $CsMgBr_3$:Ni^{2+}, calculated energies for the triplet excited states and the lowest-energy singlet excited state and parameters used to define the potential energy curves in Fig. 10 to obtain the calculated spectra shown in Fig. 11

Quantity	$MgBr_2$:Ni^{2+}	$CsMgBr_3$:Ni^{2+}
B (cm^{-1})	800	800
C (cm^{-1})	3200	3150
e_σ (cm^{-1})	3300	3300
e_π (cm^{-1})	800	800
Θ[a] (O_h) (°)	54.74	54.74
$^3T_{1g}(^3F)$ (cm^{-1})	11,243	11,227
^1E_g (cm^{-1}) (O_h)	12,278	12,086
Θ[a] (D_{3d}) (°)	56.19	52.36
^3E_g (cm^{-1})[b]	11,082	11,365
$^3A_{2g}$ (cm^{-1})[b]	11,501	10,777
^1E_g (cm^{-1}) (D_{3d})	12,274	12,075
ω_0 (cm^{-1}) (ground state)	170	170
ω_0 (cm^{-1}) (singlet excited state)	170	170
ω_0 (cm^{-1}) (triplet excited states)	155	155
ΔQ (Å) (singlet excited state)	0.0	0.0
ΔQ (Å) (triplet excited states)	0.18	0.18
γ (cm^{-1})	500	500
Γ (cm^{-1})	15	15
E_{00} $^3T_{1g}$(O_h) (cm^{-1})	9532[c]	9530[c]
E_{00} ^3E_g (O_h) (cm^{-1})	11,490[c]	11,312[c]
E_{00} ^3E_g (D_{3d}) (cm^{-1})	9371[c]	9669[c]
E_{00} $^3A_{2g}$(D_{3d}) (cm^{-1})	9791[c]	9081[c]
E_{00} ^1E_g (D_{3d}) (cm^{-1})	11,486[c]	11,301[c]

[a] Θ is the smallest angle between the trigonal axis and a Ni–Br bond. Polar coordinates (Θ, Φ) for all six ligands are (Θ, 0°), (Θ, 120°), (Θ, 240°), (180° − Θ, 60°)(180° − Θ, 180°) and (180° − Θ, 300°).
[b] States arising from $^3T_{1g}(^3F)$ in O_h point group symmetry.
[c] AOM energies were lowered by 788 cm^{-1} ($MgBr_2$:Ni^{2+}) and 774 cm^{-1} ($CsMgBr_3$:Ni^{2+}) for the calculation of the spectra in Fig. 11.

energy a set of vibronic lines separated by larger energy differences. The low-energy band contributes to the unresolved triplet band, it is not comparable in detail to experiment and not the focus here. The higher energy band shows a progression indicative of a final state with a small offset ΔQ and comparable to the detailed spectrum shown in Fig. 9b, as is the case for the singlet excited state. We therefore use the "singlet band" label to discuss the spectrum in Fig. 9b, even though such labels should be used with caution for two main reasons. First, the observation of a progression with several members indicates that the "singlet band" has significant triplet character, as can be seen qualitatively from the higher-energy adiabatic potential curves in Figs. 3 and 10. This adiabatic curve has its minimum at a nonzero, positive value along the normal coordinate axis due to spin-orbit coupling with the triplet state, a qualitative rationale for the "singlet" progression observed in the spectrum in Fig. 9b.

The spectra calculated for O_h point group symmetry with the parameter values given in Table 3 compare well with the experiment, but the progression intervals are too large, as is shown by the dotted calculated spectra in Fig. 11. A systematic variation of the model parameters reveals that the only way to improve the energy intervals without ending up with an unacceptable intensity distribution within the progression is to lower the vibrational frequency of the triplet excited state to approx-

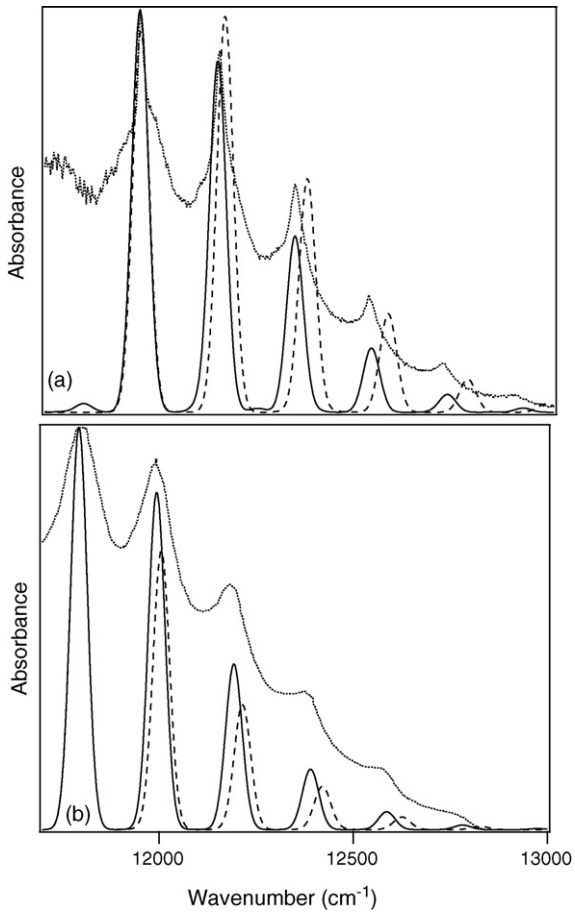

Fig. 11. Comparison of experimental and calculated absorption spectra for $MgBr_2$:Ni^{2+} (a) and $CsMgBr_3$:Ni^{2+} (b). The top traces in both panels denote experimental spectra, the two lower traces denote calculated spectra. Solid lines: spectra obtained with four coupled E_g states (D_{3d} point group symmetry, Fig. 10b), dotted lines: spectra calculated with two coupled E_g states (O_h point group symmetry, Fig. 10a.

imately 115 cm^{-1}. This reduction of 33% is too large: $NiBr_2$ shows a resolved progression with an interval of 160 cm^{-1} for the triplet excited state, lower by less than 10% than the ground state vibrational frequency, and $NiCl_2$ shows a progression interval of 251 cm^{-1}, lower by only 4% than the ground state value. We have chosen to limit the value of the vibrational frequency for the triplet excited state to a range between 90% and 100% of the ground state frequency for the calculations of absorption spectra.

It is straightforward to formally generalize this model to the D_{3d} actual point group symmetry. In this symmetry, the $^3T_{1g}(^3F)$ excited state splits into a $^3A_{2g}$ and a ^3E_g state. Three E_g spin-orbit levels arise from these states. Their energies can be estimated from the angular overlap model, using polar coordinates for the ligands derived from the crystal structure of the host lattices and choosing the angular overlap parameters e_σ, e_π, B and C to reproduce as best as possible the observed band maxima in overall spectra. The calculated energies and ligand-field parameters for this point group symmetry are given in Table 3. This approach leads to approximate energies and allows us to construct the potential energy surfaces in Fig. 10b for $MgBr_2$:Ni^{2+}. The most important difference of this model compared to Fig. 10a are the multiple E_g levels arising from the triplet excited states. The calculated spectrum is in better agreement with the experiment, providing evidence for coupling with multiple states, as illustrated in Fig. 11. The energy intervals in Table 2 are also in better agreement with the experimental data than those for the O_h approximation. The multiple E_g levels have to be treated simultaneously, not as a sum of calculations for pairs of coupled levels. Their exact energies are of lesser importance: the energy intervals calculated for the two spectra in Fig. 11 are very similar, even though the trigonal split of $^3T_{1g}$ has the opposite sign for the two host lattices, as given in Table 3.

The calculated intervals are still somewhat too large for $MgBr_2$:Ni^{2+}, in particular those at high energy. Is tempting to interpret this discrepancy as a manifestation of coupling to other E_g states higher in energy than the transitions in Fig. 10b, in analogy to the effect shown for the unresolved calculated spectra in Fig. 7 of the preceding section. More spectra are needed to analyze such effects, as a model with additional coupling parameters is vastly overparametrized for the two spectra analyzed here. Of particular interest are complexes where the spin-forbidden transition is in the middle between the two energetically close spin-allowed bands. The comparison in Fig. 11 shows that single-crystal absorption spectra confirm the importance of multiple spin-allowed transitions on the lowest-energy spin-forbidden band and its vibronic structure, involving the multiple E_g levels arising from $^3T_{1g}(^3F)$ in the D_{3d} point group symmetry of the magnesium(II) site of the two bromide host lattices.

7. Summary and conclusions

This review shows that spectroscopic effects of coupling between multiple excited states, usually neglected in the interpretation of absorption spectra, can be observed in absorption spectra of octahedral nickel(II) complexes both in solution and in the solid state. The intensity and vibronic structure of the lowest-energy spin-forbidden transition reveal the influence of multiple allowed transitions. Interference effects involving several allowed transitions can lead to a surprising intensity decrease of forbidden transitions and are a likely reason why most spin-forbidden transitions are not visible in solution absorption spectra, despite their energetic proximity to several allowed bands.

Acknowledgements

This work was made possible by research grants from the Natural Sciences and Engineering Research Council (Canada). We thank Professors Jeffrey I. Zink and Daniel Neuhauser (University of California, Los Angeles), for helpful discussions and for the computer program used to calculate spectra involving multiple coupled potential energy surfaces, Professor Hans U. Güdel and Dr. Oliver S. Wenger (Universität Bern) for helpful discussions and for the absorption spectrum of $MgBr_2$:Ni^{2+} and Marie-Christine Nolet (Université de Montréal) for several of the solution absorption spectra used here.

References

[1] C.K. Jørgensen, Acta Chem. Scand. 9 (1955) 1362.
[2] A.D. Liehr, C.J. Ballhausen, Ann. Phys. 2 (1959) 134.
[3] J. Reedijk, P.W.N.M. Van Leeuwen, W.L. Groeneveld, Rec. Trav. Chim. Pays-Bas 87 (1968) 129.
[4] O.S. Wenger, S. Bénard, H.U. Güdel, Inorg. Chem. 41 (2002) 5968.
[5] M.-C. Nolet, R. Beaulac, A.-M. Boulanger, C. Reber, Struct. Bond. 107 (2004) 145.
[6] M.-C. Nolet, A. Michaud, C. Bain, D. Zargarian, C. Reber, Photochem. Photobiol. 82 (2006) 57.
[7] D. Neuhauser, T.-J. Park, J.I. Zink, Phys. Rev. Lett. 85 (2000) 5304.
[8] J.V. Lockard, G. Valverde, D. Neuhauser, J.I. Zink, Y. Luo, M.N. Weaver, S.F. Nelson, J. Phys. Chem. A 110 (2006) 57.
[9] M.H.L. Pryce, G. Agnetta, T. Garofano, M.B. Palma-Vittorelli, M.U. Palma, Phil. Magn. 10 (1964) 77.
[10] E.I. Solomon, C.J. Ballhausen, Mol. Phys. 29 (1975) 279.
[11] G. Bussière, C. Reber, J. Am. Chem. Soc. 120 (1998) 6306.
[12] M. Triest, G. Bussière, H. Bélisle, C. Reber, J. Chem. Ed. 77 (2000) 670, http://www.jchemed.chem.wisc.edu/JCEWWW/Articles/JCENi/JCENi.html.
[13] G. Bussière, C. Reber, D. Neuhauser, D.A. Walter, J.I. Zink, J. Phys. Chem. A 107 (2003) 1258.
[14] J. Ackerman, E.M. Holt, S.L. Holt, J. Sol. State Chem. 9 (1974) 279.
[15] G.L. McPherson, G.D. Stucky, J. Chem. Phys. 57 (1972) 3780.
[16] G. Benedek, I. Pollini, L. Piseri, R. Tubino, Phys. Rev. B 20 (1979) 4303.
[17] M. Kozielski, I. Pollini, G. Spinolo, J. Phys. C: Sol. Stat. Phys. 5 (1972) 1253.
[18] C. Reber, H.U. Güdel, Inorg. Chem. 25 (1986) 1196.
[19] J. Landry-Hum, G. Bussière, C. Daniel, C. Reber, Inorg. Chem. 40 (2001) 2595.
[20] A. Abragam, B. Bleaney, Electron Paramagnetic Resonance of Transition Metal Ions, Clarendon Press, Oxford, 1970, p. 449.
[21] K.L. Bray, Top. Curr. Chem. 213 (2001) 1.
[22] D. Wexler, J.I. Zink, C. Reber, J. Phys. Chem. 96 (1992) 8757.
[23] C. Reber, J.I. Zink, Comm. Inorg Chem. 13 (1992) 177.
[24] C.E. Schäffer, C.K. Jørgensen, J. Inorg. Nucl. Chem. 8 (1958) 143.
[25] C.W. Reimann, J. Phys. Chem. 74 (1970) 561.
[26] U. Oetliker, M.J. Riley, H.U. Güdel, J. Lumin. 63 (1995) 63.
[27] E.J. Heller, Acc. Chem. Res. 14 (1981) 368.
[28] J.I. Zink, K.-S.K. Shin, Adv. Photochem. 16 (1991) 119.
[29] C. Reber, J.I. Zink, J. Chem. Phys. 96 (1992) 2681.
[30] J.I. Zink, Coord. Chem. Rev. 211 (2001) 69.
[31] T. Brunold, H.U. Güdel, in: E.I. Solomon, A.B.P. Lever (Eds.), Inorganic Electronic Structure and Spectroscopy, John Wiley & Sons, Inc., New York, 1999, p. 259.
[32] U. Oetliker, M.J. Riley, P.S. May, H.U. Güdel, J. Luminesc. 53 (1992) 553.
[33] C.K. Jørgensen, Acta Chem. Scand. 9 (1955) 405.
[34] C.K. Jørgensen, Acta Chem. Scand. 9 (1955) 1362.
[35] A. Anderson, Y.W. Lo, J.P. Todoeschuck, Spectr. Lett. 14 (1981) 105.
[36] R.W.G. Wyckoff, Crystal Structures, vol. 1, Interscience, New York, 1963, p. 268.
[37] G.L. McPherson, A.M. McPherson, J.L. Atwood, J. Phys. Chem. Solids 41 (1980) 495.